Journal of Sound and Vibration 329 (2010) 1422–1434

Contents lists available at ScienceDirect

Journal of Sound and Vibration

journal homepage: www.elsevier.com/locate/jsvi

The importance of roof shape for road traffic noise shielding in the urban environment

T. Van Renterghem *, D. Botteldooren

Ghent University, Department of Information Technology, Sint-Pietersnieuwstraat 41, B-9000 Gent, Belgium

ARTICLE INFO

Article history:
Received 10 August 2009
Received in revised form
3 November 2009
Accepted 9 November 2009
Handling Editor: A.V. Metrikine
Available online 8 December 2009

ABSTRACT

The influence of roof shape on sound propagation in a densely build-up city centre is evaluated. Road traffic noise propagation from a street canyon to an adjacent, non-directly exposed building façade is numerically studied by the finite-difference time-domain method. A large number of common and less common roof shapes were analyzed in an idealized city canyon configuration. Roof shape can be responsible for differences in road traffic noise shielding exceeding 10 dBA, averaged over the shielded façade. Therefore, roof shape can be considered as an important means to limit sound pressure levels at a quiet side; various researchers indicated that the presence of silent zones and façades may limit city noise annoyance. With increasing vehicle speed, the choice of roof shape becomes more important. The roof top height was shown to be a bad predictor of shielding efficiency in the equal-building-volume approach followed in this study.

1. Introduction

Noise annoyance in the urban environment is a major environmental problem. The main source of noise annoyance in a city is road traffic. This understanding lead to a number of large European research projects related to noise issues, aiming at scientifically support the implementation of the Environmental Noise Directive by the European Commission (2002/49/EC). A main obligation of this directive is the production of city noise maps for large European cities, in order to assess the current state of the sound environment and to locate black-points where action is needed.

In noise maps, the full complexity of the sound propagation problem in a city cannot be taken into account for reasons of computational cost. Especially the sound levels at the non-directly exposed side of a building are only a very rough estimate [1]. However, these quiet façades play an important role in the perception of noise in a city. It was found, based on large-scale surveys, that people having easy access to a quiet place near their dwellings are less highly-annoyed by noise [2,3]. Such a silent place is e.g. a backyard, or a bedroom at the non-directly exposed façade of a building. This means that city noise mapping models are often not sufficient to make a good estimation of the actual impact of environmental noise.

The study of a "city canyon" gets a lot of attention in environmental studies. Examples of air quality modeling [4–6], sound propagation [7–15], thermal comfort [16,17], etc. are numerous. A good knowledge of what is happening in such a geometry is considered to be of main importance to assess the impact of environmental stressors in the urban environment.

Sound propagation in city canyons and between adjacent city canyons is a complex problem. Streets mainly contain acoustically rigid materials, leading to strong street reverberation. Interference of reflecting sound waves between building

* Corresponding author. Tel.: +32 9 264 99 94; fax: +32 9 264 99 69.
E-mail addresses: Timothy.Van.Renterghem@intec.Ugent.be (T. Van Renterghem), Dick.botteldooren@intec.Ugent.be (D. Botteldooren).

0022-460X/$ - see front matter © 2009 Elsevier Ltd. All rights reserved.
doi:10.1016/j.jsv.2009.11.011

façades leads to the presence of modes in the canyon. Realistic façades are not fully flat, leading to an important amount of diffuse reflection. Several diffraction edges can be distinguished when sound propagates over roofs towards non-directly exposed façades. Meteorological effects like refraction by gradients in wind speed and air temperature, and turbulent scattering can significantly affect sound levels, especially at shielded locations [12]. Accurate modeling in such geometries needs full-wave numerical methods.

Recent research to decrease sound levels in (adjacent) street canyons focus mainly on the application of sound absorption [7,12–15] and strengthening the diffuse field [7–9,12–14]. Both numerical simulations and scale model studies showed the importance of such measures.

An aspect that has received little attention is roof shape. Two studies looked at the difference between saddle-backed roofs and flat roofs [18,19]. Both studies found that in a windless situation, a flat roof leads to more shielding at the back side of a building. In this paper, a wide variety of common and less common roof shapes are numerically studied, showing its influence for sound pressure levels at non-directly exposed façades for road traffic noise. To focus on the effect of roof shape, the simulations do not include meteorological effects, diffusely reflecting façades or additional absorption patches.

Full-wave methods, like the finite-difference time-domain (FDTD) method [20] that will be used in this numerical study, can indicate which roof type is beneficial for shielding. Due to the large computational cost of this type of models, only sound propagation between adjacent city canyons can be studied. City regions, on the other hand, cannot be considered. However, the simulation results in this paper can be useful as a posteriori correction factors in noise mapping software. In this way, the large gap between detailed and non-detailed propagation models can be bridged. The combination of detailed calculations to produce correction factors to be used in less-detailed and faster models is a valuable engineering approach. An application of this can be found e.g. in Ref. [21]. A city noise map was calculated by considering sound propagation over a rigid ground; the sound levels inside city canyons were calculated by using appropriate correction factors.

This paper is organized as follows. The source model and the FDTD sound propagation model are briefly discussed in Sections 2.1 and 2.2. Next, the roof shapes that are modeled and numerical parameters are given in Section 2.3. In Section 3, results are shown and discussed, with focus on the global shielding of light vehicle noise at the non-directly exposed building façade. Qualitative analysis of the shielding of some roof geometries is found in Section 4. Finally, conclusions are drawn in Section 5.

2. Numerical model

2.1. Road traffic source model

The Harmonoise/Imagine road traffic source model is a state-of-the-art model, based on a large number of measurements and outcomes of national and international research projects. An overview of this source model can be found in Ref. [22]. This model prescribes that a vehicle should be represented by two omni-directional point sources. For light vehicles (like person's cars and vans, type 1 [22]), source heights of 0.01 and 0.30 m above the road surface should be used. For heavy vehicles (like buses and trucks, type 3 [22]), these source heights are 0.01 and 0.75 m. The lowest point source is associated with rolling noise, the highest one with engine noise. There is a logarithmical relationship between rolling noise production and vehicle speed. Engine noise is linearly dependent on vehicle speed:

$$L_{\mathrm{w,rolling\ noise}}(f) = a_{\mathrm{rolling\ noise}}(f) + b_{\mathrm{rolling\ noise}}(f)\log_{10}\left(\frac{v}{v_{\mathrm{ref}}}\right) \tag{1}$$

$$L_{\mathrm{w,engine\ noise}}(f) = a_{\mathrm{engine\ noise}}(f) + b_{\mathrm{engine\ noise}}(f)\left(\frac{v\text{-}v_{\mathrm{ref}}}{v_{\mathrm{ref}}}\right) \tag{2}$$

The source power level L_w depends on the sound frequency f, vehicle speed v, and the sound generation mechanism (i.e. either rolling noise or engine noise); v_{ref} is the reference vehicle speed which equals 70 km/h. Parameters a and b are tabulated and can be found e.g. in Ref. [22]. Following the Harmonoise/Imagine source model, 80% of the rolling noise energy calculated with Eq. (1) should be attributed to the source at 0.01 m, and 20% to the source at 0.30 m. On the other hand, 80% of the engine noise energy calculated with Eq. (2) should be attributed to the higher source and 20% to the lower source. Default values of the basic model will be used for the calculations in this study. This implies that the vehicles are driving at constant speed on a dense asphalt concrete road top surface layer, and the air temperature is 20 °C.

2.2. Sound propagation model

Sound propagation in a homogeneous, still medium is described by following linear equations:

$$\boldsymbol{\nabla}\cdot p + \rho_0\frac{\partial \boldsymbol{v}}{\partial t} = \mathbf{0}, \tag{3}$$

$$\frac{\partial p}{\partial t} + \rho_0 c_0^2 \boldsymbol{\nabla}\cdot \boldsymbol{v} = 0. \tag{4}$$

In these equations, p is the acoustic pressure, v is the particle velocity, ρ_0 is the mass density of air, c_0 is the adiabatic sound speed, and t denotes time. Viscosity, thermal conductivity, molecular relaxation, and gravity are neglected.

The FDTD method is applied to solve the coupled Eqs. (3) and (4). The computational grid is built up by using the acoustic pressures and particle velocity components as unknowns. The staggered-in-time and staggered-in-space discretisation approach is chosen as described in Ref. [20]. The advantages of this numerical scheme for acoustical applications were discussed in detail in Ref. [23]. This numerical method has been validated thoroughly by comparison with measurements, analytical solutions and other numerical methods, over a wide range of (complex) acoustical applications [24–28].

In contrast to the more common frequency domain techniques like e.g. the boundary element method or the finite-element method, a time-domain method has the following important advantage. With a single simulation, the response over a wide range of frequencies can be calculated when working with a pulse-like source and when applying a Fourier transform afterwards. The Harmonoise/Imagine road traffic source model is available in 1/3 octave bands. A sufficient number of frequencies (at least 10) must be calculated to constitute the attenuation data for each 1/3 octave band. A frequency-domain technique, on the other hand, would require a new calculation for each of these frequencies.

Since the FDTD method is a volume-discretisation technique, the computational cost can be large. Furthermore, a small spatial and temporal discretisation step is needed to achieve accuracy. The calculations in this paper can however be limited to two dimensions. By doing this, it is assumed that the buildings have a constant cross-section (in the third dimension), and that a coherent line source is modelled. The source model that is used (see Section 2.1), however, is developed for point source emission. Therefore, the equivalence between sound pressure levels, expressed relative to free field sound propagation, of a coherent line source and a (single) point source [29] is assumed explicitly in the post-processing of the numerical results.

It is also important to note that the influence of source type is very limited when looking at the relative effect of a given noise reducing measure. In Ref. [15], differences of only 0.3 dB were found when modeling different abatement schemes (e.g. increasing absorption by buildings, strengthening the diffuse sound field, and increase shielding by adding small screens) for sound propagation between adjacent city canyons, in case of various source types (infinite incoherent line source, finite incoherent line source, coherent line source). In Ref. [30], the increase in noise shielding by the presence of an absorbing roof (green roof) on a building was compared for both an (infinite) incoherent (3D) and a coherent (2D) line source. The relative effect by the presence of a green roof was found to be quite independent of source type (<0.7 dB). Since this study aims at looking at the relative importance of roof shape, and given the enormous increase in computational cost when extending to three dimensional calculations, the use of two dimensional calculations is justified.

2.3. Case study and numerical parameters

Two adjacent, idealized city canyons are considered (see Fig. 1). Sound is emitted in the source canyon. Separate simulations are performed for the rolling noise and engine noise source heights. The canyons and the buildings have a

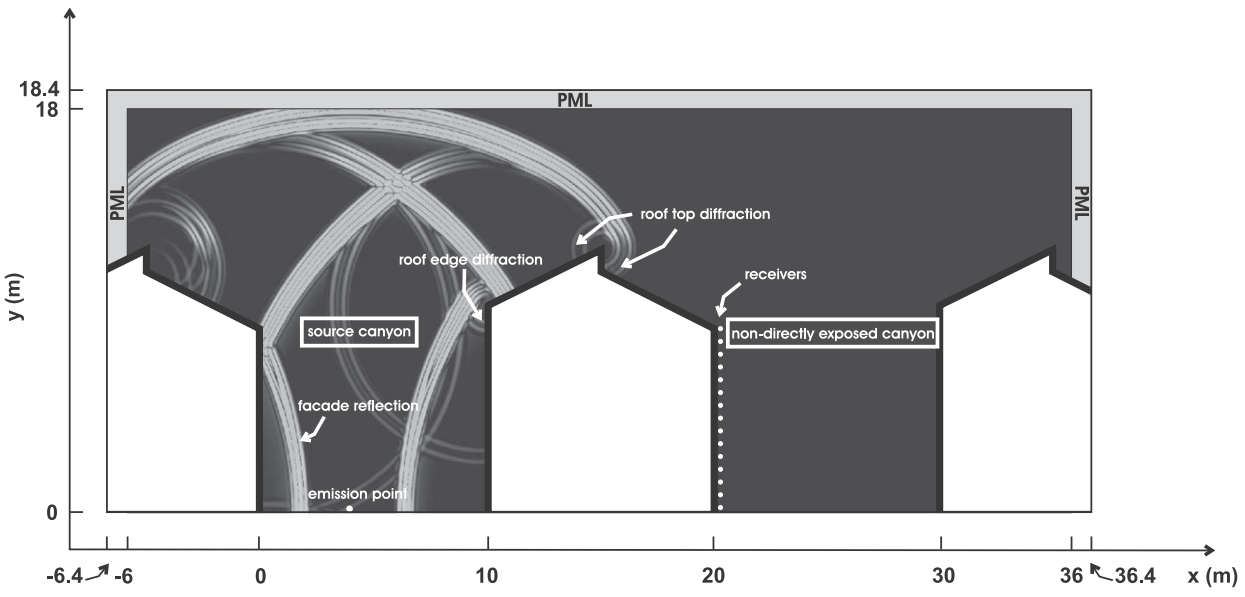

Fig. 1. Snapshot during pulse propagation from the source canyon towards the adjacent, shielded canyon. The source position and the receiver line at the non-directly exposed canyon are shown. The locations of the PML's are drawn as well. Note that the levels are shown on an arbitrary dB scale.

width of 10 m. The reference setup for the calculations is a rectangular building with a height of 10 m. The source is positioned out of the centre in the street, at 6 m from the left façade of the middle building. All surfaces are modeled as specularly reflecting. The roofs and street surface are perfectly reflecting (rigid). The vertical parts of the façades are modeled as bricks, having a reflection coefficient of 80% [31]. Receivers are located at 5 mm from the non-directly exposed façade of the middle building. At the top, right and left boundary, Perfectly Matched Layers (PML) [32] were used to efficiently absorb outgoing waves. In this way, the simulation domain can be truncated without affecting the simulation results.

In Fig. 1, a snapshot is shown during the propagation of a pulse at the emission point in the source canyon, in case of building configuration D2 (see Fig. 2). The multiple reflections at the façades, and the complex diffraction patterns near the roofs are clearly visible. The recorded pressures over time at the receiver line are the raw data that are used to calculate the shielding of a given building geometry.

An overview of the roof shapes considered is shown in Fig. 2. For some geometries, the mirror image is modeled as well. To limit the number of possibilities, all buildings in the adjacent city canyons have exactly the same roofs. Combinations of different roof shapes are not considered and would lead to a very large number of additional simulations. As an exception, a number of combinations of configuration G and its mirror image G′ are considered to form the source canyon and the non-directly exposed canyon. For a fair comparison, the volume of the buildings is kept the same when varying roof shape. This means that the maximum height of the vertical part of the façades is lower than 10 m for the alternative designs. In Table 1, an overview is given of the height of the vertical part of the façade on the left and right of the building, and also the height of the roof top. The (inner) roof slope angles of the different parts of the roofs are given as well where applicable.

Different groups of roof shapes can be distinguished. The series A1–A7 are symmetric saddle-backed roofs, with slope angles ranging from 7.5° to 52.5°, with an interval of 7.5°. The vertical parts of the façades range from 9.67 to 6.74 m, while the roof top heights range from 10.33 to 13.26 m. A number of variants of the 30° sloped saddle-backed roof (configuration A4) are considered. In a first series (configurations B1–B4), the horizontal position of the roof top is shifted along the building width (completely towards the source canyon, at 20%, 80%, and completely towards the receiver canyon). The height of the top (11.44 m) is equal to the one in the symmetric 30° sloped saddle-backed roof (configuration A4, which corresponds to a 50% shift). In a second variant (configurations C1 and C2), the roof is hanging partly over the façade, with a length of 0.5 and 1 m, respectively. In a third variant (configurations D1 and D2), a discontinuity is present in the middle of the roof, where the left and right part of the saddle-backed roof are vertically shifted over respectively 0.5 and 1 m. The roof

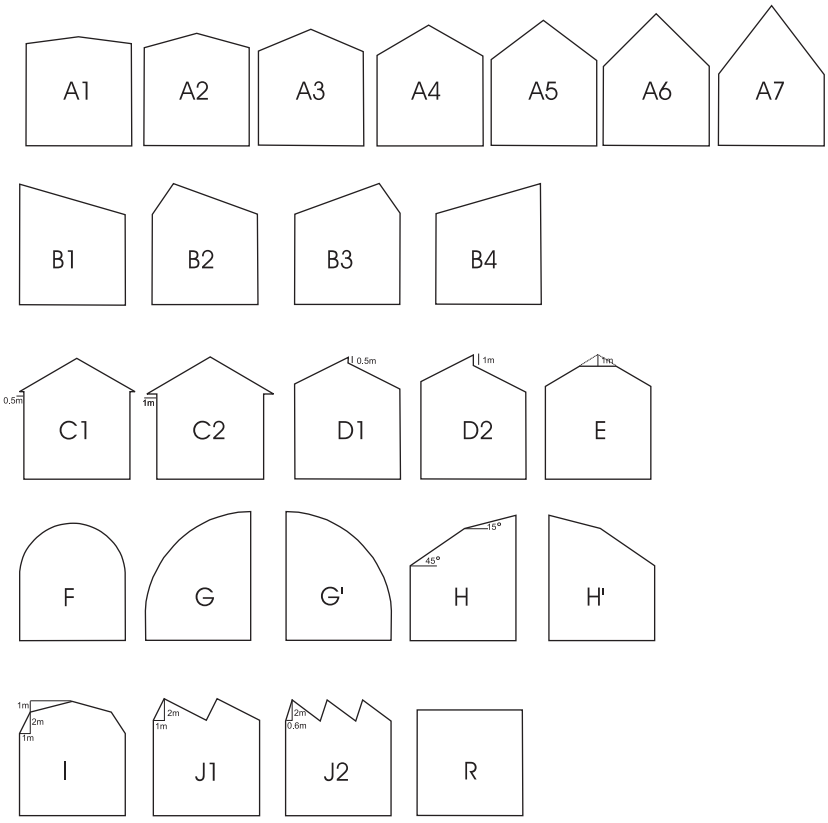

Fig. 2. Overview of the building geometries considered in this study. A more detailed description is found in the text and in Table 1.

Table 1
Overview of the configurations studied, with an indication of some relevant geometrical parameters like the height of the roof top, the height of the vertical parts of the façade, and the roof slope angles of the different parts of the roof (inner roof slope angles are given). In case there are multiple roof parts, the angles are given, going from the source to the receiver canyon.

Configuration ID	Height of roof top (m)	Height of vertical part of façade (source side) (m)	Height of vertical part of façade (receiver side) (m)	Roof slope angle(s) (deg)
A1	10.33	9.67	9.67	7.50; 7.50
A2	10.67	9.33	9.33	15.00; 15.00
A3	11.04	8.96	8.96	22.50; 22.50
A4	11.44	8.56	8.56	30.00; 30.00
A5	11.92	8.08	8.08	37.50; 37.50
A6	12.50	7.50	7.50	45.00; 45.00
A7	13.26	6.74	6.74	52.50; 52.50
B1	11.44	11.44	8.56	16.07
B2	11.44	8.56	8.56	55.22; 19.80
B3	11.44	8.56	8.56	19.80; 55.22
B4	11.44	8.56	11.44	16.07
C1	11.43	8.25	8.25	30.00; 30.00
C2	11.39	7.92	7.92	30.00; 30.00
D1	11.50	9.00	8.50	30.00; 30.00
D2	11.75	9.25	8.25	30.00; 30.00
E	10.62	8.73	8.73	30.00; 0.00; 30.00
F	11.06	6.07	6.07	
G	12.15	2.15	12.15	
G′	12.15	12.15	2.15	
H	11.85	7.02	11.85	45.00; 15.00
H′	11.85	11.85	7.02	15.00; 45.00
I	10.80	7.80	7.80	63.43; 14.04
J1	11.00	9.00	9.00	1 triangle: 63.43; 26.57
J2	11.00	9.00	9.00	1 triangle: 71.57; 40.60
R	10.00	10.00	10.00	0.00

slope angles in configurations C1, C2, D1, and D2 are all 30°. In configuration E, the 30° angle roof is truncated; the height of the roof top is 1 m lower than in case of the 30° symmetric saddle-backed roof.

A second set of roofs contains curved parts (configurations F, G, and G′), or curved roofs approached by a limited number of straight lines (configurations H, H′, and I). Configuration F has a half-cylinder top, with a diameter equal to the building width. Buildings G and G′ are constructed by using a quarter of a cylinder, with a diameter equal to two times the building width. Configurations H and H′ are asymmetric roofs consisting of a steep (slope angle of 45°) and less steep part (slope angle of 15°). The slope change occurs at half the building width. Configuration I is a symmetrical roof, having a very steep slope followed by a less steep slope, and is often called a "mansard" roof. Configurations J1 and J2 are saw-tooth roofs, consisting of respectively 2 and 3 triangles. Each triangle takes an equal part of the building width. The top of each triangle is located at 1/5 of the longest side, towards the source canyon. The heights of these triangles are all 2 m. The reference building (configuration R) has a flat roof.

This study does not intend to give a complete overview of all possible roof shapes and related parameters, although a large variety of common (and less common) roof shapes are modeled. Since the numerical simulations are performed in two dimensions, geometrical invariance in the third dimension is implicitly assumed.

The FDTD method uses a uniform, structured Cartesian grid, with square cells. The spatial discretisation step equals 0.01 m, and the time step equals 20 μs. The propagation medium (air) has a speed of sound c_0 of 340 m/s and a mass density ρ_0 of 1.2 kg/m^3. This corresponds to a Courant number of 1 [20], resulting in minimum phase errors [20], numerical stability [20], and minimal simulation time. About 32 000 time steps were needed for the acoustic pulse to complete die out in the simulation region.

3. Numerical results and discussion

The results in this section show the difference in total A-weighted traffic noise level between the different roof shapes and a rectangular building, at the moment both the passing vehicle and the receivers are located in a plane, orthogonal to the building façades. At this moment, sound pressure levels at the non-directly exposed façade are maximal. The simulated vehicle speeds range from 30 to 70 km/h. Although the higher vehicles speeds in this range are not appropriate in the source canyon considered, such a broad range is however useful to assess the effects that can be expected. Both light vehicles and heavy vehicles are considered in this evaluation.

In Fig. 3, the spectrum is shown at the shielded façade, at half building height in the reference configuration R, for a light vehicle. The spectra at different traffic speeds are depicted. With the spatial resolution of 0.01 m (see Section 2.3),

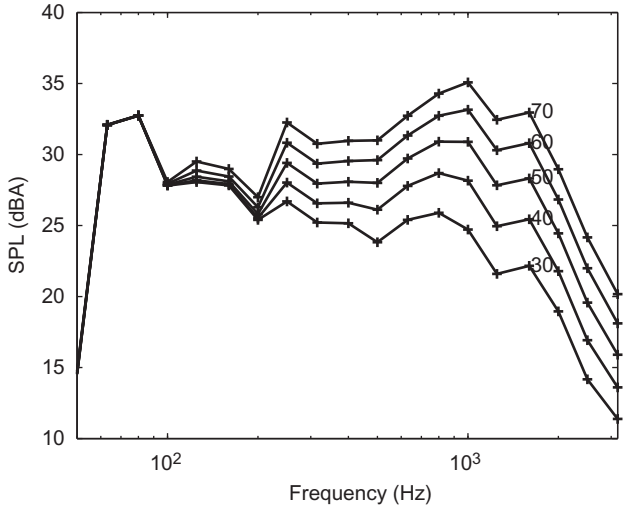

Fig. 3. Spectrum at the shielded façade, at half building height, for configuration R. The numbers on the lines indicate the speed of the light vehicle (in km/h) in the source canyon.

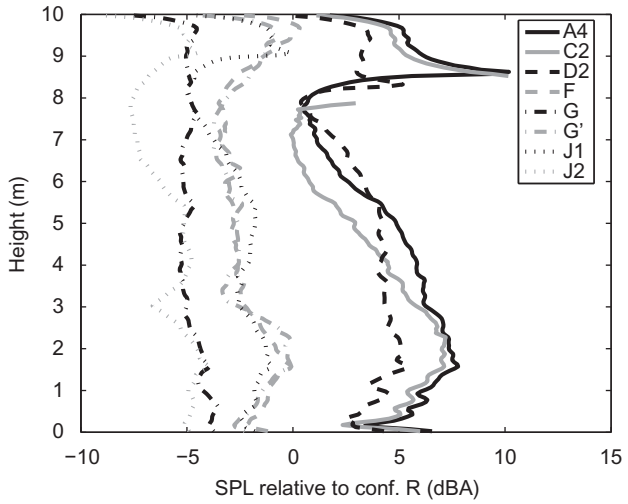

Fig. 4. Sound pressure level, relative to configuration R, for total A-weighted traffic noise along the non-directly exposed façade, for a light vehicle driving at 50 km/h in the source canyon. A selection is made of some roof shapes with an increased and decreased shielding relative to the rectangular building.

accurate calculations can be performed up to the 1/3 octave band of 3150 Hz (when obeying the "10 computational cells per wavelength"-criterion). At lower speeds, engine noise is dominant, which is characterized by low frequencies. At higher speeds, the high frequent noise production by the interaction between the tires and the road (rolling noise) becomes more important. This means that for high vehicle speeds, the high frequency part of the spectrum gives the largest contribution to the total A-weighted traffic noise levels. However, even for a vehicle speed of 70 km/h, including 1/3 octave bands up to the one with central frequency 2000 Hz is largely sufficient to calculate the total A-weighted traffic noise level at the back façade (neglecting higher 1/3 octave bands leads to an error of only 0.03 dBA). The use of an even finer spatial resolution than actually needed to calculate traffic noise levels at a shielded side results in a further reduction of FDTD phase errors, and in an accurate representation of sloped parts in the staircase approach followed.

In Fig. 4, the difference in A-weighted road traffic noise between a selection of building geometries and the reference building is shown at each height, in case of a light vehicle driving at 50 km/h in the source canyon. This figure gives a clear view of the behavior of the different geometries with height along the façade under study. Negative values indicate an improved shielding relative to the rectangular building (configuration R). Since the line of receivers crosses the overhanging part of the building in case of configuration C2, no data is presented at some heights.

The box plots in Fig. 5 give a more general view of the shielding of the different roof shapes. All vehicles speeds, ranging from 30 till 70 km/h, are included. Light vehicles and heavy vehicles are considered separately. Receiver heights range

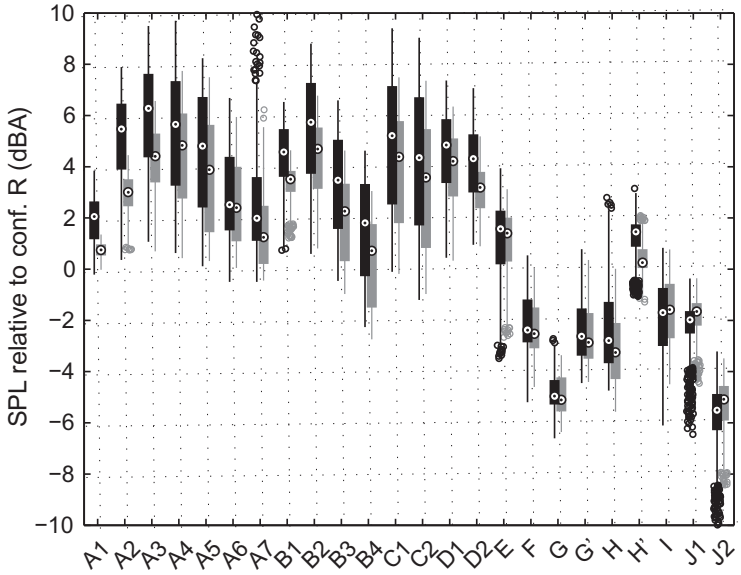

Fig. 5. Boxplots showing the sound pressure level, relative to configuration R, for total A-weighted traffic noise, along the shielded façade (from ground level up to 7.5 m). Vehicle speeds ranging from 30 to 70 km/h are considered. The boxplots for light vehicles are shown in black, for heavy vehicles in gray.

from street level up to a height of 7.5 m. Total A-weighted sound pressure level differences between a certain roof shape and the rectangular building (configuration R) at each corresponding height along the non-directly exposed façade of the central building were calculated. Although the data itself cannot be considered as a continuous distribution, the use of box plots is an interesting way to present the results in a concise and compact way. The middle circle in the box indicates the median of the data. The box is closed by the first and third quartile. The whiskers extend to 1.5 times the interquartile distance above the maximum value inside the box, and to 1.5 times the interquartile distance below the minimum value inside the box. Data points that fall outside these limits are indicated with the open circles. This representation gives a clear indication of the variation of the shielding efficiency along the façades and with different vehicle speeds. Such plots give a general view of what can be expected at the shielded side in case of a certain roof shape.

When looking at a specific height along the façade under consideration, differences amounting up to 20 dBA are found for light vehicles and up to 15 dBA for heavy vehicles. When considering the median on these data, roof shape can be responsible for differences exceeding 10 dBA. Roof shape can therefore be considered as an important means to limit sound pressure levels from road traffic at a quiet side.

Two main groups can be considered. A first group (configurations A to E) has a shielding median that is lower than the rectangular building (configuration R). The interquartile distances are large. A second group (configurations F to J) has a shielding that is better than a flat roof, except for configuration H′. There, the variation with speed and height is usually more limited. It can further be observed that the noise shielding for light and heavy vehicles is very similar in this second group. In the first group, on the other hand, larger differences can be found. A more detailed analysis of series A1–A7 and B1–B4 is found further in this paper. The use of an overhanging roof (configurations C1 and C2) results in a limited improvement relative to configuration A4, which has the same roof slope angle. An overhanging (horizontal) part of the roof of 1 m is better than an overhanging part of 0.5 m. A vertical shift between the left and right part of the roof (configurations D1 and D2) improves shielding somewhat. A larger discontinuity is preferable. Configuration E, where part of the roof is flat, is an even better choice.

The use of curved roofs seems to be a good choice to achieve silence at the back-façade of a dwelling. The median of the difference in shielding between a half-cylinder top (configuration F) and a flat façade (configuration R) is near -2.5 dBA for both light and heavy vehicles. A quarter-cylindrical roof, with the curved part facing the source canyon (configuration G) increases shielding. Its mirror image (configuration G′) gives 2 dBA less shielding. Configurations H and H′ have similarities with G and G′—but now the curves are approached by two straight lines. This results in less shielding. It is again better to face the curved part towards the source canyon. In case of a right-facing roof top, the median now becomes even larger than in the reference configuration. The mansard roof (configuration I) performs slightly worse than the half-cylinder roof. Saw-tooth roofs (configurations J1 and J2), and especially the one with 3 saw-points (configuration J2), result in a significant improvement in shielding relative to a flat roof (configuration R).

Additional simulations were performed with combinations of G and G′ for light vehicles. When the curved parts of both façades face the source canyon (combination G′–G–G, when going from the left to the right), a similar distribution is obtained as in Fig. 3 for configuration G (i.e. actually the combination G–G–G). However, the median is reduced to -6.9 dBA relative to configuration R. On the other hand, combination G–G′–G′ performs significantly worse, and only gives

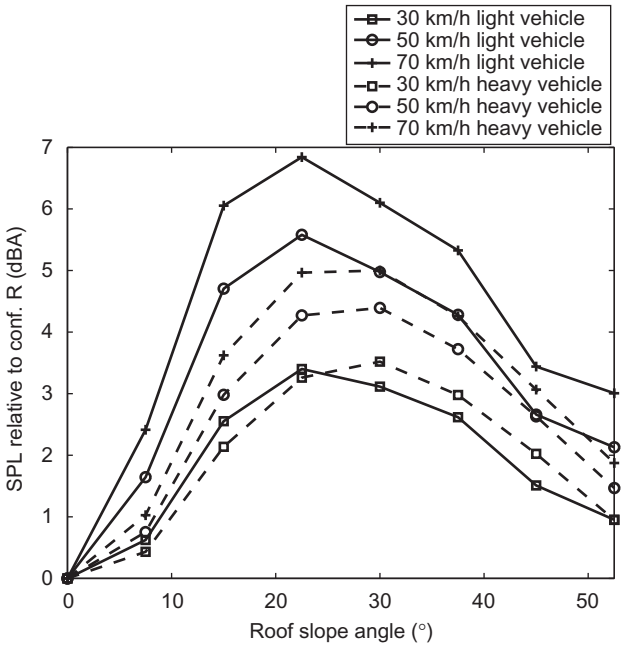

Fig. 6. Averaged sound pressure level, relative to configuration R, of total A-weighted traffic noise along the shielded façade (from ground level up to 7.5 m), in function of the roof slope angle for symmetric saddle-backed roofs (configurations A1–A7). Results are shown for both light and heavy vehicles.

a similar shielding as in the reference configuration. The combinations could be ranked as follows, with increasing sound pressure level median relative to configuration R (or a decreasing degree of shielding): G′–G–G (−6.9 dBA) > G–G–G (−5.0 dBA) > G–G′–G (−3.8 dBA) > G′–G′–G′ (−2.6 dBA) > G′–G–G′ (−1.3 dBA) > G–G′–G′ (0.3 dBA). These numerical results clearly show that considering combinations of building geometries in the adjacent canyons might further help to optimize shielding towards a quiet façade.

Two series are studied in more detail. Series A (configurations A1–A7) represents buildings with different roof slope angles, in case of a symmetric saddle-backed roof. In Fig. 6, the averaged sound pressure level, relative to the reference configuration, along the shielded façade is shown in function of roof slope angle. Three vehicle speeds are considered, namely 30, 50, and 70 km/h. Results for both light and heavy vehicles are depicted. With increasing vehicle velocity, the influence of roof slope angle on shielding becomes more important. The reason for this lies in the traffic source spectrum: with increasing vehicle speed, high frequencies become more and more dominant. The shielding at high frequencies is more sensitive to small changes in building geometry, and this in contrast to low frequencies. When changing roof slope angle, a maximum is found near 22.5° for light vehicles, and near 30° for heavy vehicles (see Fig. 6). At this point, shielding is smallest. With increasing vehicle speed, this maximum becomes more pronounced, especially for light vehicles. A good choice is either a very low roof slope angle (flat roof), or a very high slope angle. For light vehicles, there is no preference between very high or low slope angles at 30 km/h, while a flat roof stays preferable at higher speeds.

In a second series B (B1–B4), the (horizontal) roof top location is studied. In Fig. 7, the effect of roof top location on shielding efficiency is depicted. The top height is taken equal to the one of the 30° symmetric saddle-backed roof (configuration F4). As long as the top position is present at the left half of the building (configurations B1, B2, and F4), differences in shielding are within 1 dBA for both light and heavy vehicles. Once past the middle, there is an important increase in shielding at all vehicle speeds. As in series A, the effect of vehicle speed is more pronounced for light vehicles than it is for heavy vehicles.

The height of the roof top is clearly not a good indicator of shielding efficiency. For a vehicle speed of 30 km/h, a flat roof (configuration R) and the 52.5° symmetric saddle-backed roof (configuration A7) result in similar degree of shielding, while the difference in roof top height is large. In series B, all roofs have an equal top height, and equal façade heights. Nevertheless, differences up to 4 dBA are found for a vehicle speed of 70 km/h. Qualitative explanation by means of ray tracing for these two series can be found in Section 4.

In Table 2, a ranking is made of the shielding capacity of the different roof shapes considered, for 3 vehicle speeds. The receiver heights range from 0 to 7.5 m. In Table 3, the shielding efficiency is calculated in 3 zones along the non-directly exposed façade (from ground level to 2.5 m, from 2.5 to 5 m, and from 5 to 7.5 m). A constant vehicle speed of 50 km/h is then used. Such tables are interesting to fine-tune the roof shape choice, based on the prevailing vehicle speed in the street canyon, or based on the distribution of people along the building height. With increasing vehicle speed, the difference between the configurations leading to the largest and lowest amount of shielding increases. This span over the 24 roof

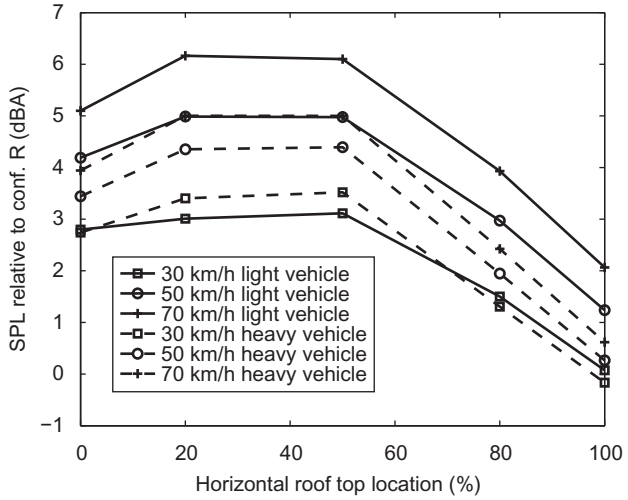

Fig. 7. Averaged sound pressure level, relative to configuration R, of A-weighted traffic noise along the shielded façade (from ground level up to 7.5 m), in function of the horizontal location of the roof top (configurations B1, B2, A4, B3 and B4). Results are shown for both light and heavy vehicles. The roof top height is constant. A roof top location of 0% means that the roof top is present completely at the left of the façade (configuration B1); 100% means a shift completely towards the shielded façade (configuration B4).

Table 2
Average shielding along the shielded façade (from ground level up to 7.5 m), relative to a rectangular building (configuration R), for all roof shapes considered (see Fig. 2). A ranking is performed, for 3 vehicles speeds in the source canyon. Light vehicles and heavy vehicles are considered separately. The values in between brackets are the corresponding standard deviations.

Rank number	Shielding relative to rectangular building (in dBA) at 30 km/h (Height: 0.0–7.5 m)				Shielding relative to rectangular building (in dBA) at 50 km/h (Height: 0.0–7.5 m)				Shielding relative to rectangular building (in dBA) at 70 km/h (Height: 0.0–7.5 m)			
	Light vehicle		Heavy vehicle		Light vehicle		Heavy vehicle		Light vehicle		Heavy vehicle	
1	J2	−4.8 (0.7)	J2	−5.1 (0.8)	J2	−5.5 (1.0)	J2	−5.4 (1.0)	J2	−6.1 (1.2)	J2	−5.6 (1.2)
2	G	−4.4 (0.6)	G	−4.7 (0.8)	G	−4.8 (0.5)	G	−5.0 (0.7)	G	−5.0 (0.7)	G	−5.2 (0.8)
3	H	−3.1 (0.8)	H	−3.3 (1.0)	H	−2.6 (1.4)	H	−3.2 (1.3)	G′	−2.7 (1.1)	H	−3.1 (1.6)
4	I	−2.4 (0.8)	G′	−2.3 (1.1)	G′	−2.3 (1.1)	G′	−2.6 (1.1)	J1	−2.2 (1.1)	G′	−2.8 (1.2)
5	J1	−2.3 (0.5)	F	−2.1 (0.9)	J1	−2.2 (0.7)	F	−2.3 (1.0)	F	−2.1 (1.3)	F	−2.4 (1.3)
6	F	−2.1 (0.7)	I	−1.9 (1.0)	I	−2.2 (1.3)	J1	−1.8 (0.7)	H	−2.1 (1.9)	J1	−1.7 (1.0)
7	G′	−1.8 (1.1)	J1	−1.9 (0.5)	F	−2.2 (0.9)	I	−1.7 (1.3)	I	−1.9 (1.8)	I	−1.5 (1.6)
8	B4	0.1 (1.3)	B4	−0.2 (1.5)	E	0.9 (1.4)	B4	0.3 (1.7)	H′	1.5 (0.6)	H′	0.6 (0.6)
9	E	0.1 (1.0)	H′	0.3 (0.7)	H′	1.1 (0.6)	H′	0.4 (0.6)	E	1.5 (1.7)	B4	0.6 (1.8)
10	A1	0.6 (0.4)	A1	0.4 (0.2)	B4	1.2 (1.6)	A1	0.8 (0.2)	B4	2.1 (1.9)	A1	1.0 (0.2)
11	H′	0.7 (1.0)	E	0.6 (1.1)	A1	1.6 (0.5)	E	1.0 (1.4)	A1	2.4 (0.5)	E	1.3 (1.6)
12	A7	1.0 (1.4)	A7	1.0 (1.2)	A7	2.1 (1.6)	A7	1.5 (1.3)	A7	3.0 (1.8)	A7	1.9 (1.4)
13	B3	1.5 (1.2)	B3	1.3 (1.4)	A6	2.7 (1.5)	B3	1.9 (1.6)	A6	3.4 (1.6)	B3	2.4 (1.8)
14	A6	1.5 (1.3)	A6	2.0 (1.5)	B3	3.0 (1.6)	A6	2.6 (1.6)	B3	3.9 (1.8)	A6	3.1 (1.7)
15	C2	1.9 (2.0)	A2	2.1 (0.5)	D2	3.8 (1.0)	A2	3.0 (0.5)	D2	4.7 (1.1)	D2	3.5 (1.0)
16	D2	2.5 (0.7)	C2	2.4 (2.2)	C2	3.9 (2.5)	D2	3.1 (0.9)	C2	5.1 (2.7)	A2	3.6 (0.5)
17	A2	2.6 (0.8)	D2	2.5 (0.8)	D1	4.1 (1.3)	C2	3.3 (2.4)	D1	5.1 (1.5)	C2	3.9 (2.6)
18	A5	2.6 (1.6)	B1	2.7 (0.6)	B1	4.2 (0.6)	B1	3.4 (0.5)	B1	5.1 (0.7)	B1	3.9 (0.4)
19	C1	2.6 (1.8)	A5	3.0 (1.9)	A5	4.3 (2.0)	A5	3.7 (2.1)	A5	5.3 (2.2)	A5	4.3 (2.3)
20	D1	2.8 (1.1)	C1	3.0 (2.0)	C1	4.5 (2.3)	D1	3.9 (1.5)	C1	5.7 (2.6)	D1	4.3 (1.6)
21	B1	2.8 (0.7)	A3	3.3 (1.0)	A2	4.7 (0.8)	C1	3.9 (2.3)	A2	6.1 (0.7)	C1	4.5 (2.5)
22	B2	3.0 (1.2)	D1	3.3 (1.2)	A4	5.0 (2.1)	A3	4.3 (1.2)	A4	6.1 (2.3)	A3	5.0 (1.4)
23	A4	3.1 (1.6)	B2	3.4 (1.2)	B2	5.0 (1.7)	B2	4.4 (1.4)	B2	6.2 (2.0)	A4	5.0 (2.3)
24	A3	3.4 (1.1)	A4	3.5 (1.7)	A3	5.6 (1.4)	A4	4.4 (2.0)	A3	6.8 (1.6)	B2	5.0 (1.6)

shapes modeled for light vehicles are 8.2, 11.1, and 12.9 dBA for vehicle speeds of 30, 50 and 70 km/h, respectively. For heavy vehicles, these values are 8.6, 9.8, and 10.6 dBA. However, when ranking the shielding of different roof configurations for both light and heavy vehicles, at various vehicle speeds and for different zones along the façade, similar lists were obtained. This shows that the optimal roof shape choice is only weakly dependent on vehicle type, vehicle speed, and the zone considered along the façade.

Table 3
Average shielding along the shielded façade (at a vehicle speed of 50 km/h), relative to a rectangular building (configuration R), for all roof shapes considered (see Fig. 2). Light vehicles and heavy vehicles are considered separately. A ranking is performed for different regions along the shielded façade: from ground level to 2.5 m, from 2.5 to 5 m, and from 5 to 7.5 m. Values for the global performance over the full façade height (from street level to 7.5 m) are shown in the last column. The values in between brackets are the corresponding standard deviations.

Rank number	Shielding relative to rectangular building (in dBA) at 50 km/h (Height: 0.0–2.5 m)				Shielding relative to rectangular building (in dBA) at 50 km/h (Height: 2.5–5.0 m)				Shielding relative to rectangular building (in dBA) at 50 km/h (Height: 5.0–7.5 m)				Shielding relative to rectangular building (in dBA) at 50 km/h (Height: 0.0–7.5 m)			
	Light vehicle		Heavy vehicle		Light vehicle		Heavy vehicle		Light vehicle		Heavy vehicle		Light vehicle		Heavy vehicle	
1	J2	−4.7 (0.3)	J2	−4.7 (0.4)	J2	−5.4 (0.5)	G	−5.4 (0.3)	J2	−6.5 (0.9)	J2	−6.6 (0.8)	J2	−5.5 (1.0)	J2	−5.4 (1.0)
2	G	−4.1 (0.3)	G	−4.1 (0.4)	G	−5.2 (0.1)	J2	−4.8 (0.4)	G	−5.0 (0.2)	G	−5.4 (0.4)	G	−4.8 (0.5)	G	−5.0 (0.7)
3	J1	−1.7 (0.4)	H	−1.6 (0.4)	H	−2.9 (0.5)	H	−3.5 (0.6)	H	−3.9 (0.5)	H	−4.6 (0.5)	H	−2.6 (1.4)	H	−3.2 (1.3)
4	I	−1.4 (0.7)	G′	−1.4 (0.8)	G′	−2.5 (0.7)	G′	−2.9 (1.0)	I	−3.8 (0.9)	G′	−3.5 (0.2)	G′	−2.3 (1.1)	G′	−2.6 (1.1)
5	G′	−1.2 (0.9)	J1	−1.4 (0.5)	F	−2.4 (0.4)	F	−2.7 (0.5)	G′	−3.2 (0.4)	I	−3.3 (0.6)	J1	−2.2 (0.7)	F	−2.3 (1.0)
6	F	−1.1 (0.5)	F	−1.0 (0.5)	J1	−2.2 (0.3)	J1	−1.6 (0.1)	F	−3.0 (0.2)	F	−3.1 (0.2)	I	−2.2 (1.3)	J1	−1.8 (0.7)
7	H	−0.9 (0.4)	I	−0.7 (0.7)	I	−1.4 (0.4)	I	−1.1 (0.5)	J1	−2.8 (0.8)	J1	−2.5 (0.8)	F	−2.2 (0.9)	I	−1.7 (1.3)
8	H′	1.2 (0.8)	A1	0.6 (0.3)	H′	0.7 (0.3)	H′	0.2 (0.2)	B4	−0.8 (0.7)	B4	−1.8 (0.6)	E	0.9 (1.4)	B4	0.3 (1.7)
9	A1	1.3 (0.5)	H′	0.9 (0.8)	A7	1.1 (0.5)	A7	0.7 (0.6)	E	−0.6 (1.3)	E	−0.6 (1.2)	H′	1.1 (0.6)	H′	0.4 (0.6)
10	E	1.8 (0.7)	B4	1.7 (0.6)	A1	1.6 (0.1)	A1	0.8 (0.1)	C2	0.9 (0.9)	B3	−0.1 (0.7)	B4	1.2 (1.6)	A1	0.8 (0.2)
11	B4	2.3 (0.7)	E	1.7 (0.6)	E	1.7 (0.2)	B4	1.0 (0.8)	B3	1.0 (0.9)	H′	0.2 (0.4)	A1	1.6 (0.5)	E	1.0 (1.4)
12	A7	2.8 (0.6)	A7	2.4 (0.7)	B4	2.3 (0.7)	E	1.8 (0.2)	A6	1.4 (1.0)	C2	0.3 (0.9)	A7	2.1 (1.6)	A7	1.5 (1.3)
13	B3	3.9 (0.8)	A2	2.8 (0.8)	A6	2.6 (1.0)	A6	2.5 (1.0)	H′	1.4 (0.5)	A1	0.9 (0.1)	A6	2.7 (1.5)	B3	1.9 (1.6)
14	B1	3.9 (0.9)	B3	3.1 (0.7)	B3	4.0 (0.4)	B3	2.8 (0.6)	C1	1.7 (1.2)	C1	1.1 (1.1)	B3	3.0 (1.6)	A6	2.6 (1.6)
15	A6	4.0 (1.0)	B1	3.2 (0.7)	D2	4.3 (0.2)	A2	3.0 (0.1)	A5	1.9 (0.7)	A6	1.1 (0.7)	D2	3.8 (1.0)	A2	3.0 (0.5)
16	D2	4.2 (0.8)	D2	3.7 (0.8)	B1	4.5 (0.2)	D2	3.4 (0.3)	A1	2.0 (0.4)	A5	1.2 (0.6)	C2	3.9 (2.5)	D2	3.1 (0.9)
17	A2	4.3 (1.2)	A6	4.4 (0.9)	A2	4.8 (0.2)	B1	3.7 (0.1)	A7	2.4 (2.3)	A7	1.3 (1.7)	D1	4.1 (1.3)	C2	3.3 (2.4)
18	D1	4.7 (0.9)	A3	4.7 (0.9)	C2	4.8 (1.2)	C2	4.3 (1.2)	A4	2.5 (1.3)	A4	1.9 (1.3)	B1	4.2 (0.6)	B1	3.4 (0.5)
19	A5	5.6 (1.2)	D1	4.7 (0.8)	D1	4.9 (0.4)	A5	4.4 (1.1)	D1	2.9 (1.3)	D1	2.2 (1.0)	A5	4.3 (2.0)	A5	3.7 (2.1)
20	B2	5.6 (1.1)	B2	4.8 (0.9)	A5	5.4 (0.9)	D1	4.8 (0.5)	D2	3.0 (0.9)	D2	2.2 (0.7)	C1	4.5 (2.3)	D1	3.9 (1.5)
21	C2	6.0 (1.2)	C2	5.4 (1.1)	C1	5.7 (0.8)	A3	4.9 (0.1)	B2	3.3 (1.6)	B2	2.9 (1.4)	A2	4.7 (0.8)	C1	3.9 (2.3)
22	A3	6.1 (1.1)	C1	5.6 (1.0)	A4	6.0 (0.6)	C1	5.2 (0.9)	B1	4.1 (0.4)	A2	3.1 (0.3)	A4	5.0 (2.1)	A3	4.3 (1.2)
23	C1	6.3 (1.1)	A5	5.6 (1.0)	B2	6.1 (0.1)	B2	5.4 (0.1)	A3	4.3 (1.5)	A3	3.2 (1.3)	B2	5.0 (1.7)	B2	4.4 (1.4)
24	A4	6.5 (1.0)	A4	5.8 (0.9)	A3	6.4 (0.3)	A4	5.6 (0.6)	A2	5.1 (0.4)	B1	3.5 (0.2)	A3	5.6 (1.4)	A4	4.4 (2.0)

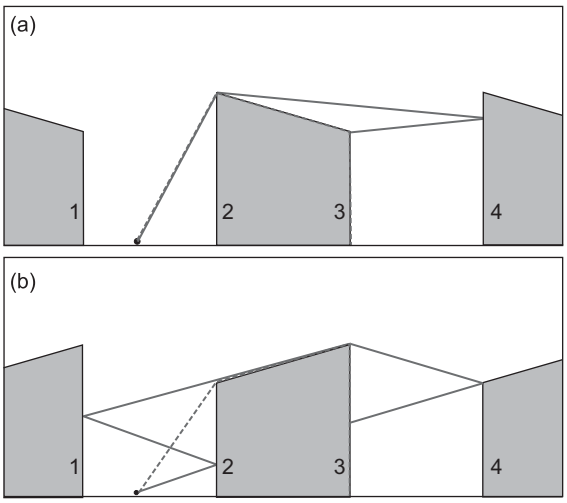

Fig. 8. Sound ray analysis in configuration B1 (a) and B4 (b). The shortest single-edge diffraction path is shown (full lines), together with the pure diffraction path (dashed line, in absence of façade reflections).

4. Qualitative analysis

Qualitative analysis of sound propagation between adjacent city canyons, involving multiple reflections and diffractions in both the source canyon and receiver canyon, is often very difficult. It was already indicated by analyzing both measurements and simulations that the shortest sound paths (those arriving earliest in time) are usually not the ones containing the most energy [14].

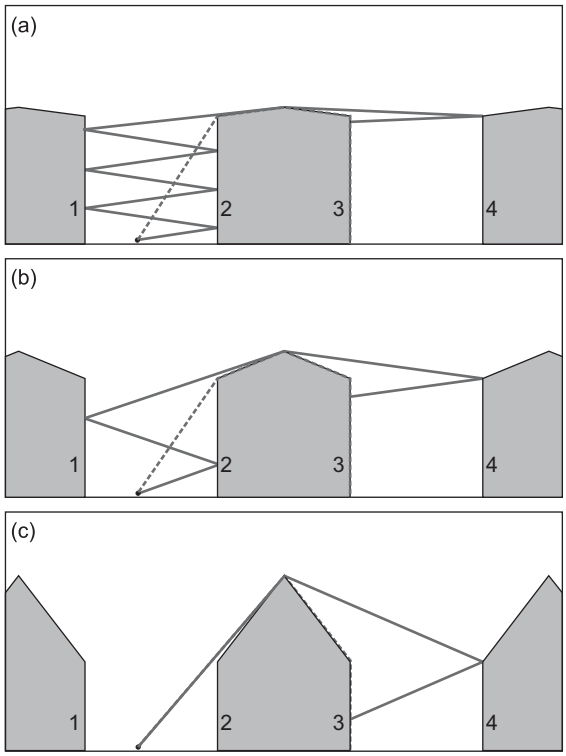

Fig. 9. Sound ray analysis in configurations A1 (a), A3 (b), and A7 (c). The shortest single-edge diffraction path is shown (full lines), together with the pure diffraction path (dashed line, in absence of façade reflections).

In Figs. 8 and 9, sound ray analysis is performed to explain the behavior as found in Figs. 6 and 7. Only specular reflection is considered, which means that the angle of incidence equals the angle of reflection. A ray model is in essence a high-frequency approach. A diffracting edge can be modelled as a secondary sound source. Although its limitations, such analysis is interesting to qualitatively explain the difference in shielding between various roof shapes.

An important indicator of the degree of shielding is whether there are sound paths towards the shielded façade, demanding single-edge diffraction only. In the street canyon setup studied, such sound paths are only possible when reflections on façades 1 and 4 are involved (see Figs. 8 and 9). Because of the interaction of sound with the (partly absorbing) façades, and the extra distance travelled (caused by geometrical spreading of sound waves), there is additional energy loss for such paths. However, this decrease in energy is subordinate to the decrease in sound pressure level caused by a pure diffraction path. What happens in the receiver canyon is also important in this respect. A single-edge diffraction path needs a reflection on façade 4 (in the receiver canyon) as well. In some situations, only part of the façade under study (façade 3) can be reached by such reflections. Sound at this non-illuminated part (by reflections on façade 4) may only come from multiple diffractions (e.g. diffraction at the roof top, followed by diffraction near the right edge of the building).

Applied to configuration B1, single edge diffraction, followed by a reflection on façade 4 can totally illuminate façade 3. In configuration B4, single edge diffraction is only possible when 2 reflections are involved in the source canyon. This leads to less intense sound arriving at the roof top edge. Furthermore, only half of façade 3 is illuminated by a subsequent reflection on façade 4. This analysis shows why averaged shielding in configuration B4 is superior to B1.

Sound ray analysis in configuration A1 shows that a large number of reflections are needed in the source canyon to reach the building top, with a corresponding high amount of energy loss. On the other hand, the shielded façade 3 is almost totally illuminated by reflections on façade 4. In configuration A7, single edge diffraction is possible without façade reflections in the source canyon. However, the relative large shielding can be attributed due to the fact that sound can only reach a large part of façade 3 (the upper part) by a subsequent diffraction at the top of the shielded façade. The illumination of façade 3 by reflections on façade 4 is indeed very poor, as illustrated in Fig. 9c. Configuration A3 lies in between these two extremes. A few reflections in the source canyon suffice, while the reflections following single-edge diffraction on façade 4 can reach a large part of façade 3. This leads to limited shielding compared to configurations A1 and A7.

The course of the shortest path (the pure-diffraction-path) is another indicator of shielding. Edge diffraction leads to more energy loss when the diffraction angle increases. Another parameter is the number of diffraction edges. The saw-tooth roof J2 is optimal among the configurations studied: there are sharp changes in angles between the different parts of the roof, and the number of diffraction points is large.

Note however that in case of sound propagation over an individual row of houses (not in a city canyon setup), there is only a pure diffraction path (no façade reflections are involved) to reach receivers at the shielded façade. Additional simulations showed that in such a situation, the roof slope angle (in series A) should be as low as possible. With increasing angle, shielding decreases. When evaluating series B in case of an individual row of houses, the centre point of the roof top is optimal when it is in the middle of the building. The exact source location plays now a more important role. In such an individual row of houses setup, however, roof shape is less important since sound pressure levels at the shielded façade are already quite low, compared to the street canyon configuration.

5. Conclusions

The numerical results in this paper show that roof shape has an important influence on road traffic noise propagation from a street canyon to a nearby non-directly exposed façade. When looking at a specific height along such a façade, differences in peak level amount up to 20 dBA for light vehicles and up to 15 dBA for heavy vehicles when changing roof shape. Averaged over the full façade, roof shape can be responsible for differences exceeding 10 dBA. Roof shape can therefore be considered as an important means to limit sound pressure levels at a quiet side. With increasing vehicle speed, the choice of roof shape becomes more important. This effect is more pronounced for light vehicles than for heavy vehicles. The roof top height was shown to be a bad predictor of shielding efficiency in the equal-volume approach followed in this study. Qualitative sound ray analysis showed that the roof shape in the receiving canyon is important as well. Ranking the optimal roof shape is only weakly dependent on vehicle type, vehicle speed, and the zone considered along the shielded façade.

Due to the computational cost, the full-wave model used for the detailed evaluation of roof shape in this study cannot be used for noise mapping purposes. On the other hand, in common noise mapping software, the building geometry is often largely simplified, and only approximate diffraction formulas are used, with focus on a fast evaluation. Roof details are not accounted for. The gap between these two types of models is therefore large. This implies a risk that city planners and noise action plan responsibles will not use roof shape as a control measure since it remains "invisible" in noise maps. The simulation results in this paper can be a starting point for a posteriori correction factors to noise mapping results. However, such correction factors will be model-specific since each noise mapping model has their own approaches and calculation rules to estimate diffraction.

This numerical study has some limitations. In the current study, only the effect of roof shape is considered. Additional absorption, or making the sound field more diffuse, may improve shielding as well [12–15]. Besides, meteorological effects can increase or decrease noise shielding [12]. It is important to note that these parameters might interact with roof shape; the combined effect is often not a simple addition of the separate effects [7,12].

Combinations of roof shape in nearby canyons were not studied in detail in this paper, given the large number of possibilities. However, the simulations considering different combinations of a quarter-cylinder roof (configuration G) and its mirror image (configuration G′) indicated that combining different roof shapes in nearby canyons might help to further improve noise shielding.

Geometrical variation along the length of the canyons is not considered in the 2D simulations. When looking at the influence of roof shape on the maximum level received by a passing car in a street, as was done in this paper, geometrical variance along the street is expected to be of minor importance (as long as there are no gaps in between the houses).

As a last remark, the sound received at a shielded place in a city does not only come from a nearby canyon, but also from sources further away [21]. The effect of roof shape on this type of sound contribution is probably limited.

References

[1] T. Kihlman, M. Ögren, W. Kropp, Prediction of urban traffic noise in shielded courtyards, *Proceedings of Internoise 2002*, Dearborn, MI, USA.
[2] E. Öhrstrom, Psycho-social effects of traffic noise exposure, *Journal of Sound and Vibration* 151 (1991) 513–517.
[3] E. Öhrstrom, A. Skanberg, H. Svensson, A. Gidlöf-Gunnarsson, Effects of road traffic noise and the benefit of access to quietness, *Journal of Sound and Vibration* 295 (2006) 40–59.
[4] C. Mensink, G. Cosemans, From traffic flow simulations to pollutant concentrations in street canyons and backyards, *Environmental Modelling and Software* 23 (2008) 288–295.
[5] X. Li, C. Liu, D. Leung, Numerical investigation of pollutant transport characteristics inside deep urban street canyons, *Atmospheric Environment* 43 (2009) 2410–2418.
[6] Y. Huang, X. Hu, N. Zeng, Impact of wedge-shaped roofs on airflow and pollutant dispersion inside urban street canyons, *Building and Environment* (2009), doi:10.1016/j.buildenv.2009.03.024.
[7] K. Horoshenkov, D. Hothersall, S. Mercy, Scale modelling of sound propagation in a city street canyon, *Journal of Sound and Vibration* 223 (1999) 795–819.
[8] J. Kang, Sound propagation in street canyons: comparison between diffusely and geometrically reflecting boundaries, *Journal of the Acoustical Society of America* 107 (2000) 1394–1404.
[9] J. Picaut, L. Simon, A scale model experiment for the study of sound propagation in urban areas, *Applied Acoustics* 62 (2001) 327–340.
[10] T. Le Pollès, J. Picaut, M. Bérengier, C. Bardos, Sound field modeling in a street canyon with partially diffusely reflecting boundaries by the transport theory, *Journal of the Acoustical Society of America* 116 (2004) 2969–2983.
[11] M. Ögren, W. Kropp, Road traffic noise propagation between two dimensional city canyons using an equivalent sources approach, *Acta Acustica united with Acustica* 90 (2004) 293–300.
[12] T. Van Renterghem, E. Salomons, D. Botteldooren, Parameter study of sound propagation between city canyons with a coupled FDTD-PE model, *Applied Acoustics* 67 (2006) 487–510.

[13] M. Hornikx, J. Forssén, The 2.5-dimensional equivalent sources method for directly exposed and shielded urban canyons,, *Journal of the Acoustical Society of America* 122 (2007) 2532–2541.
[14] M. Hornikx, J. Forssén, A scale model study of parallel urban canyons, *Acta Acustica united with Acustica* 94 (2008) 265–281.
[15] M. Hornikx, J. Forssén, Noise abatement schemes for shielded canyons, *Applied Acoustics* 70 (2009) 267–283.
[16] J. Herbert, G. Johnson, A. Arnfield, Modelling the thermal climate in city canyons, *Environmental Modelling and Software* 13 (1998) 267–277.
[17] D. Pearlmutter, P. Berliner, E. Shaviv, Integrated modeling of pedestrian energy exchange and thermal comfort in urban street canyons, *Building and Environment* 42 (2007) 2396–2409.
[18] T. Van Renterghem, D. Botteldooren, Numerical simulation of sound propagation over rows of houses in the presence of wind, *Proceedings of International Congress on Sound and Vibration* (*ICSV*) *2003*, Stockholm, Sweden, pp. 1381–1388.
[19] D. Heimann, Three-dimensional linearised Euler model simulations of sound propagation in idealised urban situations with wind effects, *Applied Acoustics* 68 (2007) 217–237.
[20] D. Botteldooren, Finite-difference time-domain simulation of low-frequency room acoustic problems, *Journal of the Acoustical Society of America* 98 (1995) 3302–3308.
[21] P. Thorsson, M. Ögren, W. Kropp, Noise levels on the shielded side in cities using a flat city model, *Applied Acoustics* 65 (2004) 313–323.
[22] H. Jonasson, Acoustical source modelling of road vehicles, *Acta Acustica united with Acustica* 93 (2007) 173–184.
[23] T. Van Renterghem, D. Botteldooren, Prediction-step staggered-in-time FDTD: an efficient numerical scheme to solve the linearised equations of fluid dynamics in outdoor sound propagation, *Applied Acoustics* 68 (2007) 201–216.
[24] R. Blumrich, D. Heimann, A linearized Eulerian sound propagation model for studies of complex meteorological effects, *Journal of the Acoustical Society of America* 112 (2002) 446–455.
[25] T. Van Renterghem, D. Botteldooren, Numerical simulation of the effect of trees on downwind noise barrier performance, *Acta Acustica united with Acustica* 89 (2003) 764–778.
[26] T. Xiao, Q. Liu, Finite difference computation of head-related transfer functions for human hearing, *Journal of the Acoustical Society of America* 113 (2003) 2434–2441.
[27] L. Liu, D. Albert, Acoustic pulse propagation near a right-angle wall, *Journal of the Acoustical Society of America* 119 (2006) 2073–2083.
[28] A. Bockstael, T. Van Renterghem, D. Botteldooren, W. D'Haenens, H. Keppler, L. Maes, B. Philips, F. Swinnen, B. Vinck, Verifying the attenuation of earplugs in situ: method validation on human subjects including individualized numerical simulations, *Journal of the Acoustical Society of America* 125 (2009) 1479–1489.
[29] T. Van Renterghem, E. Salomons, D. Botteldooren, Efficient FDTD-PE model for sound propagation in situations with complex obstacles and wind profiles, *Acta Acustica united with Acustica* 91 (2005) 671–679.
[30] T. Van Renterghem, D. Botteldooren, Numerical evaluation of sound propagating over green roofs, *Journal of Sound and Vibration* 317 (2008) 781–799.
[31] ISO 9613-2, Acoustics—attenuation of sound during propagation outdoors—Part 2: General method of calculation. International Organization of Standardization, Geneva, Switzerland, 1996.
[32] J. Berenger, A perfectly matched layer for the absorption of electromagnetic waves, *Journal of Computational Physics* 114 (1994) 185–200.